The Effects of Dry and Wet Rock Surfaces on Shear Behavior of the Interface Between Rock and Cemented Paste Backfill

Zhanguo Xiu[1], Shuhong Wang[1✉], Yingchun Ji[2], Feili Wang[1✉], Fengyu Ren[1], Van-Tuan Nguyen[1]

[1] School of Resources and Civil Engineering, Northeastern University, China.
[2] School of Science, Engineering & Environment, University of Salford, UK.
✉ Corresponding Author: wangshuhong@mail.neu.edu.cn (Tel: +86 13478143390) & wangfeili109@126.com (Tel: +86 13940267431)

Abstract

Cemented Paste Backfill (CPB) technology has been effective in using the tailings to refill the underground cavities. The wet or dry rock surface can significantly affect the stability of the CPB-Rock interface, and the shear load-bearing capacity of CPB-Rock interface always reflects the overall stability of the filled underground cavities. Therefore, clear understanding on the shear behavior of the CPB-Rock interface with wet or dry rock surface is very important. To investigate the shear behavior of CPB-Rock interface with different rock surfaces (wet and dry), an apparatus for shear tests at CPB-Rock interface was constructed by modifying the servo-controlled GCTS (Geotechnical Consulting & Testing System) loading frame. Over 72 CPB-Rock samples with dry and wet rock surfaces were tested under four confining pressures (0, 50, 100 and 150 kPa) and different curing time (1, 3, 7 days). The findings show that, under the same confining pressure and curing time, the shear strength of the CPB-Rock interface with the dry rock surface is much larger than that of the wet one. Furthermore, with the increase of the curing time under a same confining pressure, the increase of shear strength on the dry rock surface is also larger than that of the wet one due to the presence of water film on the wet rock surface. The shear strength is enhanced with the increase of confining pressure. Further, the testing results were analyzed within the framework of the Mohr-Coulomb criterion, which comply with the corresponding theoretical curve. It is concluded that the dry rock surface is essential to the stability of the filled underground cavities. In case of wet environment for the underground cavities, it is important to find ways to dry the rock surface before carrying out back filling using CPB method.

Keywords Tailings; Rock; Cemented Paste Backfill; CPB-Rock interface; Shear behavior

1 Introduction

Mining was and still is one of the most important economic activities in the world. However, the mining of metal mines tends to produce large amounts of solid wastes (tailings, waste rock, etc.) and underground cavities [1-3]. These solid wastes piling up on the ground surface can be harmful for the surrounding environment, and the resulted underground cavities left behind can cause geological instability to the area, posing a potential threat to people's lives [4-6]. Backfilling has been widely used in the past to mitigate such issues, namely using the potentially harmful solid wastes to refill the cavities created during the mining activities [7-9]. Backfilling method can effectively: *a*. ensure the stability of the stope; *b*.

minimize environmental damages to the surroundings; *c*. increases the mine productivity by improving recovery rates [10,11].

During the last decades, Cemented Paste Backfill (CPB) has become a popular backfilling method due to its simple operating procedures and environmental advantages [12-14]. Generally, CPB is mainly composed of tailings, water and binder (Ordinary Portland Cement is usually used) [15,16]. According to the fluidity of the CPB slurry, its solid content of mixed slurry can reach 70%~85% by weight. The binder usually in a proportion of 3% to 10% by weight, and sometimes the proportion up to 10% are designed to get early strength [17]. After the homogenous slurry is mixed on the mine surface, it is transported to the underground cavities by pumping or gravity.

Once the CPB is filled back into the underground cavities, its mechanical properties play a key role for the stability of the stope [1,18,19]. In addition to the strength requirements (usually refers to unconfined compressive strength, UCS) of the backfilled body, a key factor which needs to be carefully considered is the shear strength produced by the directly contact between the backfilled materials and its surrounding rock walls [17,20]. When the CPB is filled into the underground cavities, the arching effect is created due to the solidification and bonding effects between the CPB and the surrounding rock walls. The schematic diagram of the interaction between rock wall and CPB is shown in Fig. 1(a). The arching effect has been confirmed by many researchers [21-24]. Also, some scholars have examined the influence of the mechanical behavior of CPB-Rock interface on the arching effect. Liu et al.' [25,26] works indicate that the vertical and horizontal normal stresses decreased as the interface shear strength increased. And when the shear strength of the CPB-Rock interface is lower than that of the backfill, the stress estimation in backfilled stopes must be made by accounting for the mechanical parameters of interface. Yan et al.' [27] work also indicates that the mechanical behaviors at the interface between the backfill and the surrounding rock have a greater effect on the arching effect (especially the interfacial friction angle at the interface plays a key parameter). Therefore, the interfacial shear mechanical behaviors of the CPB-Rock tend to play a critical role in the backfill arching. Meanwhile, the vertical stress in the backfilled body (shown in Fig. 1b) is significantly less than its self-weight stress due to the arching effect [28,29]. This characteristic bears the great significance for the deep well filling. The existence of the arching effect also means that the design of the CPB can significantly reduce the amount of binder materials required leading to the reduced cost of producing CPB [30]. Also, with the CPB body, the load comes from the surrounding rock walls can be effectively transmitted, then the stress was redistributed. And it can helps to control the movement of the surrounding rock wall and minimize the occurrence of rockburst [31].

There is Fig.1

It is widely accepted that understanding the interfacial shear behavior of the CPB-Rock interface is of great significance to the stability of the backfilled body. A few experimental investigations have been carried out to understand or assess the shear behavior of the CPB-Rock interface in relation to different factors such as temperature, sulphate and binder content

[32-35]. What has been overlooked in this area is the shear behavior of the CPB-Rock interface under dry and wet rock surfaces. In actual practices, due to the continuous infiltration from the surface water or groundwater into the underground cavities [36-38], the mining cavities can have both dry and wet surrounding rock surfaces at the time of backfilling (as shown in Fig. 2). These two different rock surface conditions will inevitably have important impacts on the shear mechanical behavior of the CPB-Rock interface. The focus of this research is therefore to experimentally investigate the shear behavior of the CPB-Rock interface under such conditions with different curing time.

There is Fig.2

2 Experimental methodology

2.1 Testing material selection and specimen preparation

2.1.1 CPB slurry

Usually, CPB slurry are made by uniformly mixed tailings, water and binder (Ordinary Portland Cement was used as a binder in this study). The tested CPB slurry have a water-to-binder ratio (w/c) at 4.75 and the binder content used is 7.55 wt.%. The slump of the fresh paste mixture, measured by using a slump test in accordance with ASTM C143/C143M-15a [39], was equal to 18 cm, which is a slump value mostly used in many backfilling operations.

It is worth noting that the natural tailings contain abundant chemical components (e.g., sulphate) that can have complex effects on the shear behavior of the CPB-Rock interface [32,40,41]. The silica tailings (with 99.8% SiO_2) used in this study can effectively eliminate the interference of these complicated factors (e.g. sulphate). These silica based artificial tailings were widely used in laboratory in examining the mechanical behavior of CPB [11,32,33,42]. For the same purpose, distilled water was used instead of natural water in mixed CPB slurry. The main chemical element of the silica tailings is shown in Table 1. And the various physical forms and element composition of silica tailings used in this study are provided in Fig. 3.

Table 1 Main chemical element of the silica tailings used.

Element unit	Si (wt.%)	Al (wt.%)	Na (wt.%)	Fe (wt.%)	Pb (wt.%)	S (wt.%)	K (wt.%)
Silica tailings	99.8	0.1	<0.01	<0.01	-	-	-

There is Fig.3

Also, the particle sizes of silica tailings were assessed using a Mastersize 2000 laser particle size analyser. The particle size distribution of silica tailings used in the study is close to the average particle sizes of tailings from 7 mines randomly selected across different regions in China (Fig. 4). It can be seen from Fig. 4 that the fine particle contents (particle sizes are less than 20μm) of the silica tailings and the average of 7 mines tailings are 39.07% and 41.96%, respectively. According to the Unified Soil Classification System (USCS), these two types of tailings can be considered as fine-grained soils [43,44]. Table 2 shows the key physical properties of the two types tailings. It can be seen from the test results that the particle size

distributions of the two tailings are relatively close. Therefore, artificial tailings (silica tailings) are considered to be an alternative to natural tailings for the experimental research in this study. The silica tailings (used in this study) with the coefficient of uniformity C_u and coefficient of curvature C_c are approximately 17.886 and 1.251, respectively.

There is Fig.4

Table 2 Physical properties of the tailings.

Parameters	Unit	Silica tailings	7 mine tailings
D_{10} (particle size at 10% passing)	μm	2.550	2.413
D_{30} (particle size at 30% passing)	μm	12.064	9.860
D_{50} (particle size at 50% passing)	μm	32.193	32.300
D_{60} (particle size at 60% passing)	μm	45.609	55.804
D_{90} (particle size at 90% passing)	μm	144.855	210.917
$C_u=D_{60}/D_{10}$ (coefficient of uniformity)	-	17.886	23.126
$C_c=(D_{30})^2/(D_{10}*D_{60})$ (coefficient of curvature)	-	1.251	0.722
$\Delta=(D_{90}-D_{10})/D_{50}$ (relative span factor)	-	4.420	6.455
Fines content (<20μm)	%	39.07	41.96
Classification	-	Fine-grained soil	Fine-grained soil

2.1.2 Rock

Red sandstone, as a typical rock wall, is distributed broadly in metal mines all over China. Therefore, the rock samples used in the study were red sandstone with an average uniaxial compressive strength (UCS) of 27.5MPa and natural water absorption of 5.1%, respectively. The cylindrical rock core specimens with size of 50 mm × 100 mm (diameter × height) were initially obtained from a large red sandstone using a specific rock coring process. Then all the core specimens were cut into two parts along with the height direction using the rock cutter, as shown in Fig. 5a. And then the shear surface of the rock samples was polished in order to eliminate the influence of roughness on testing results. Fig. 5b shows the surface of the red sandstone sample magnified 500 times. The surface of the red sandstone particles looks rough, and mainly composed of various elements such as Si, O and Al (shown by higher counts in Fig 5c). Figs. 5d and 5e show the optical microscopic images (obtained using the Stereo Microscope-SMZ745T, Nikon) of the red sandstone sample under dry and wet conditions used in this study. It can be clearly seen that the pore sizes of the red sandstone sample are approximately several hundred microns (Figs. 5d and 5e). However, the water film layer can be obviously observed in the wet rock surface, and the pores are completely filled with water (Fig. 5e).

There is Fig.5

To accurately reflect the shear surface roughness of the red sandstone, the shear surface of the red sandstone sample (as shown in Fig. 5a) is scanned by handheld 3D laser scanner (Artec 3D Space Spider, Artec, USA) to obtain point cloud data represented by X, Y and Z axis coordinates. Then, the point cloud data are imaged using MATLAB software. Fig. 6 is a diagram illustrating the shear surface roughness of the red sandstone sample, while Fig. 6a is a contour of the shear surface

and Fig. 6b is a three-dimensional illustration. In order to quantitatively characterize the roughness of the shear surface of the red sandstone sample, 5 section lines were taken from the shear plane along the shear direction (as shown in Fig. 6a). The surface roughness index, i.e., joint roughness coefficient (JRC) proposed by Barton and Choubey [45], can then be calculated using the evaluation method from Du et al., [46,47]. The calculation equation is defined as:

$$JRC = 49.2114 e^{\frac{29L_0}{450L_n}} \arctan(8R_A) \quad (1)$$

Where, L_0 (mm) is the horizontal length of each profile line; L_n (mm) is the length of the n^{th} segment of the surface profile line; $R_A = \Delta h/L_0$ is the ratio of the relative altitude Δh to L_0 of each profile line.

The roughness of the shear surface has an important influence on the shear mechanical behavior of CPB-Rock interface. The calculation results (JRC values of the given 5 section lines) show that along the shear direction, all the JRC values of the rock surface roughness are less than 1.5 (as shown in Fig. 6a). Therefore, the shear surface has a small fluctuation along the shear direction and can be regarded as a “smooth” surface (a smooth surface is defined when JRC is between 0 and 2 by Shen et al., [48]). And for a “smooth” surface, the influences from the small fluctuation of rock surface roughness on the testing results can be ignored.

There is Fig.6

2.1.3 Sample preparation

Each tested sample consists of two parts, which are CPB and the red sandstone. All the samples are cured in a special plastic cylindrical mold with the size of 50 mm × 100 mm (diameter × height). As mentioned previously, the water-to-binder ratio (w/c) and binder content of CPB were held at 4.75 and 7.55 wt.%, respectively. The cylindrical red sandstone samples with size of 50 mm × 100 mm (diameter × height) were cut into two parts along with the height direction. Half of the sandstone sample was placed in an 80℃ drying oven to dry to the state the sample’s weight is no longer changing. And the other part was placed in distilled water and soaked to a constant weight (about 48 hours). Then, the sandstone sample was placed into the mold and the uniform CPB slurry was casted subsequently. To prevent the loss of moisture during the curing, all samples were sealed. The tested samples were placed in an environmentally controlled chamber to maintain temperature at 20 ± 2℃ curing for 1, 3 and 7 days. It should be noted that understanding the shear behavior of the CPB-Rock interface at early stages after backfill is of special importance for the opening of barricades, and thereby, reducing mining cycle time and increasing mining efficiency and production. Therefore, the curing time from 1 to 7 days were selected in this study. The completed samples are shown in Fig. 7.

There is Fig.7

2.2 Testing apparatus and scheme

2.2.1 Experimental apparatus

In order to investigate the shear behavior of the CPB-Rock interface, a modified method for shear test of CPB-Rock interface was proposed in this paper (Fig. 8). The testing apparatus used in this study is modified from servo-controlled GCTS (*Geotechnical Consulting & Testing System, BST Instruments Limited Co., Beijing, China*). Fig. 8a is an actual diagram of the testing system. The modified apparatus adopted a specially designed shear module of type L to achieve the direct shear test under a constant confining pressure (Fig. 8b). The shear module of type L consisted of a pair of L-shaped shear blocks and a pair of spacers, which filled in the missing space of the shear blocks. The spacers are soft materials with a small compressive strength (the maximum compressive strength less than 5 kPa). This compressive strength is much smaller than the shear stress of each tested sample. Therefore, it can be assumed that the load is fully applied to the tested sample. And the influence of the rubber spacer on the testing results can be ignored. Normal stress σ_n was applied on the CPB-Rock interface using hydraulic water, where σ_n was always equal to the confining pressure σ_c. The axial force F applied on the shear module of type L could trigger shear dislocation of the interface. The power source of this testing device comes from dry compressed air (1 MPa). The testing sample was wrapped with a rubber membrane and the hydraulic chamber provides a constant confining pressure (σ_c) for the sample during the test.

The similar experimental principle has been used to determine the shear behavior of different materials interface [49,50]. Compared to the traditional shear-testing method (the direct shear devices), the advantages of the modified method for testing the shear behavior of the CPB-Rock interface are: *a*. a more uniform pressure will be provided using confining pressure (σ_c, *Ref:* Fig. 8b) than single normal stress (σ_n); *b*. when the confining pressure σ_c is zero, the test result is truly representing the initial cohesion (c) of the CPB-Rock interface (avoided the gravity effect on the interface).

There is Fig.8

2.2.2 Testing scheme

To obtain the shear parameters (e.g., cohesion c, friction angle φ) and strength envelope of the CPB-Rock interface, all the samples were subjected to shear test after curing for 1, 3 and 7 days under different confining pressures (σ_c). Four confining pressures (0 kPa, 50 kPa, 100 kPa and 150 kPa) were considered based on in-situ measurement of the pressures in backfilled underground cavities [51,52]. For each test, a constant confining pressures is applied on the sample, then the CPB-Rock interface is sheared at a constant shear rate of 0.5 mm/min for a maximum displacement of 5 mm. The tested results were monitored and saved automatically by using a computer software. In addition, to ensure the reliability of the tested results, each test was repeated at least three times. Collectively over 72 samples have been tested in this study. The planned experiments with various test conditions are shown in Table 3.

Table. 3 The planned experiments and testing conditions.

Rock surface	Binder content, $B_{wt\%}$ (%)	Solid content, $C_{wt\%}$ (%)	*w*/*c* ratio	Curing time	Confining pressures, σ_c (kPa)
Wet	7.55	75	4.75	1, 3 and 7 days	0, 50, 100 and 150 kPa
Dry	7.55	75	4.75	1, 3 and 7 days	0, 50, 100 and 150 kPa

Note: $B_{wt\%} = 100*M_{binder}/M_{dry\text{-}tailings}$; $C_{wt\%} = 100*M_{soild}/M_{total}$. Where, M_{binder} is the mass of binder; $M_{dry\text{-}tailings}$ is the mass of dry tailings; M_{soild} is the mass of dry solids (binder + tailings) and M_{total} is the total mass of CPB (binder + tailings + water).

3 Results and discussion

In this section, typical shear test results for different CPB-Rock interfaces will be discussed. The test results are presented by three categories: *a.* the typical displacement vs Shear stress curves; *b.* typical CPB-Rock interface failure mode; and *c.* the shear strength envelopes, which can visually display the shear parameters (e.g., cohesion, *c* and frication angle, φ) of the different CPB-Rock interfaces. In the meanwhile, the shear test results are also explained by using the different macroscopic failures of CPB-Rock interface as well as micro-structure analysis.

It should be noted that the "differential settlement" was caused by the volume shrinkage during the hydration and consolidation process. The shear area of each test sample would be changed due to the variable differential settlement (as shown in Figs. 7 and 9). And the changes of shear areas will directly affect the testing results. Therefore, the shear height was measured by using a Vernier caliper before each sample was subjected to a shear test. And the differential settlement will be considered in the calculation of the shear strength. The shear strength of each sample can be expressed as:

$$\tau = \frac{F}{A} = \frac{F}{D(H-h)} \tag{2}$$

Where, τ is the shear stress, F is vertical force applied on each CPB-Rock sample, A is the shear area, D is the diameter of sample (50 mm in this paper), H is the height of sample (100 mm in this paper), h is the differential settlement. It should be noted that the differential settlement (h, as shown in Fig. 9) is caused by uneven shrinkage of the CPB slurry during the curing time.

There is Fig.9

3.1 Effect of dry and wet rock surface on shear behavior of CPB-Rock interface

Fig. 10 shows the typical curves for the shear stress and the shear displacement of the CPB-Rock interfaces with different rock surfaces (wet and dry, cured 1 day, with a confining pressure of 50 kPa). It should be noted that before the start of each shear test, the loading system applies a stress of 5 kPa to the tested sample, which ensures that the loading bar can be in close contact with the tested sample. Therefore, the Shear stress vs. Shear displacement curves do not start from the origin (0,0) of the coordinate axis (as shown in Fig. 10). It can be clearly seen that, regardless the difference of the peak stress of the two curves, the trends of the two curves are clearly consistent. At the initial stage of loading, as the shear displacement increases, the shear stress rapidly increases to the peak stress point. After the peak point, the shear stress gradually decreases to the residual stress with the shear displacement increases. And the consistent strain softening characteristic of the CPB-

Rock interface was exhibited in the tested curves. It also can be observed from the Fig. 10, the shear strength (represented by the maximum shear stress: 48.32 kPa for dry surface and 25.79 kPa for wet surface) and shear stiffness (50 kPa/mm for dry surface and 28.57 kPa/mm for wet surface) of the dry rock surface, are significantly higher than those of the wet rock surface. It is also noticeable that the shear displacements required to reach the peak shear stress of the dry and wet surfaces are different (1.31 mm for dry surface, 1.01 mm for wet surface), and the interfacial residual stress of the dry rock is higher than that of wet rock surface.

There is Fig.10

The shear strength of the CPB-Rock interface is primarily determined by the properties of its interface. Since the CPB slurry contains a large amount of water (water-to-cement ratio (w/c) = 4.75 in this study), and the rock surface has a large number of pore structures (*Ref*: Fig. 5d), which are much larger than the size of the cement particles. When the slurry is in contact with the different rock surfaces (wet or dry) with such pore structures, it exhibits different interactions at the different interfaces, as shown in Fig. 11. When the slurry is in contact with the dry sandstone surface, the slurry from cement has been immersed in the pores and capillary tubes of the rock surface due to surface tension and capillary action (as shown in Fig. 11a). Therefore, the adhesion force will be gradually formed at the interface between the cement colloid and the rock. However, for the wet sandstone surface, its surface pores are filled with water already (*Ref*: Fig. 5e). Also, when the slurry is in contact with the wet sandstone surface, the slurry does not embed a large amount into the rock, as shown in Fig. 11(b). Therefore, due to the different interactions, the interfacial shear strength of the CPB-Rock interface with the wet rock surface is significantly smaller than that of the dry rock interface.

There is Fig.11

To clearly illustrate the different interactions at the different interfaces described above, a scanning electron microscope (SEM) was used to examine the interfacial topography and distribution of elements for both dry and wet cases using cement paste with water-to-cement ratio (w/c) = 1. It should be noted that there is a large amount of Si element in the red sandstone used in this study (green points in Fig. 12). Moreover, CPB slurry is mainly composed of a mixture of artificial tailings (with 99.8% SiO_2), binder (P.O. 42.5) and water. The binder content is only 7.55 wt%. Therefore, CPB slurry also contains a large amount of Si element. If CPB slurry is used directly to verify the different dispersal models proposed in Fig.11, the tested results will be very inconspicuous (Si element will cover the entire picture). However, if cement paste is used instead of CPB slurry, the interaction between the slurry and the rock surface (with wet and dry conditions) can be clearly seen. For the above reasons, the cement paste with w/c=1 will be more suitable for verifying the different dispersal models.

During the hydration process for cement, the main hydration products are the calcium silicate hydrate (C-S-H) and calcium hydroxide (C-H), which are the essential binding products in the hardened CPB [33,53]. It can be seen from Fig. 12 (images

produced by SEM) that the distribution of calcium element (red points) on the two different sandstone surfaces (dry and wet) is different. For the dry sandstone surface, due to the capillary action, the cement particles are absorbed into the pores of the sandstone surface and the hydration products (e.g., C-S-H, C-H) were produced in the pores. This led to a dense distribution of calcium element in the pores along the dry sandstone surface. And, the boundary between the dry sandstone and the cement paste is not clear (as shown in Fig. 12a). This embedded contact mode significantly improves the shear strength of the interface.

However, for the wet sandstone surface, due to the obvious water film on the surface (*Ref*: Fig. 5e), the capillary phenomenon is not obvious, and the cement particles can not be smoothly embedded in the pores of the wet sandstone surface. The excess water at the surface also increases the water-to-cement ratio (w/c) of the slurry at the interface, which has a negative effect on the shear strength of the interface. This can be clearly seen from Fig. 12b that the boundary of calcium element between the cement paste and the wet sandstone surface is much clearer than that of the dry rock surface. The SEM graphics on the wet rock surface indicate that the cement particles are not well embedded. This is very detrimental to the shear strength of interface. And due to the presence of the water film on the wet rock surface, cracks are more likely to occur at the interface.

There is Fig.12

Fig. 13 shows the typical shear stress versus the shear displacement curves for the CPB-Rock interface with wet and dry rock surfaces under different confining pressures (cured for 1 day). These curves illustrate the shear strain hardening and softening characteristics of the CPB-Rock interface. Fig. 13a shows the shear displacement versus the shear stress curves on wet rock surface. The curves clearly show the strain softening characteristic under lower confining pressure (0 kPa or 50 kPa). The yield fluctuation region is obvious under the higher confining pressure (100 kPa or 150 kPa). After the yield fluctuation region (shown by the dotted circle), the shear stress of the CPB-Rock interface continues to rise to the peak stress along with the increase of the shear displacement, which is clearly characterized by the shear strain hardening. It also can be seen from the Fig. 13a that the CPB-Rock interface needs more shear displacement under large confining pressures to reach the peak stress. This is due to the fact that the increase of confining pressures at the CPB-Rock interface resulted in an increased contact area between the rock surface and the CPB particles, hence the increased frictional resistance between the CPB particles and the rock surface. Similar observations were also made by Nasir & Fall [17] and Fang & Fall [33].

There is Fig.13

Fig. 13b shows the shear displacement versus the shear stress curves at the dry rock surface. Clearly, the curves at the dry rock surface are somewhat different from that of the wet rock interface. Especially, the curves exhibit a double peak shear stress under the higher confining pressures (100 kPa and 150 kPa). This multi-peak shear stress curves are also observed in

other studies (e.g, Nasir and Fall [17]; Shen et al [48]; Fang and Fall [33]). Due to the two different rock surfaces (wet and dry), the failure morphology of the shear interface will be different. Therefore, the macroscopic adhesion failure morphology of the CPB-Rock interface are used to examine the characteristics of multi-peak shear stress.

Fig. 14 shows the fracture morphology of the CPB-Rock interface (cured 1 day; confining pressure = 150 kPa). The interfacial shear failure morphology of the wet rock surface appears as an unbonded plane failure (Fig. 14a). While, the shear failure morphology of the interface at the dry rock surface shows a large area of adhesion, and the adhesion area exceeds 60% of the whole shear area (Fig. 14b). The form of failure with adhesion (Fig. 14b) indicates that the development of micro-cracks occurs during the failure process at the CPB-Rock interface. When the curve reaches the first peak stress point, a micro-destruction zone has appeared at the CPB-Rock interface. After the stress redistribution, the shear stress increases with the increase of the shear displacement, and then reaches the second peak stress point. Therefore, it is precisely because of this development of micro-destructive zone that the phenomena of multi-peak shear stress curves occur.

There is Fig.14

A closer inspection of Fig. 13 shows that the peak shear stress of the dry rock surface is significantly greater than that of the wet rock surface. And during the test for the dry rock surface, due to the continuous accumulation of shear energy at the CPB-Rock interface, a sudden release of the interfacial shear energy may have occurred to result a significant stress drop (e.g., 0 kPa and 100 kPa on Fig. 13b). This obvious stress drop may directly lead to complete separation of the CPB-Rock interface (e.g., 0 kPa), or it may result in a stress redistribution such that the shear stress continues to increase to the secondary peak (e.g., 100 kPa).

Fig. 15 shows the correlation between the peak shear stresses and the confining pressures for 1 day curing at the CPB-Rock interface for both wet and dry conditions. The two fitted lines on the graph represent the corresponding shear strength envelopes. Regardless the differences of the rock surface (wet or dry), the shear strength envelopes of the tested samples are consistent with the Mohr-Coulomb failure criterion (Eq.3). Therefore, using the Mohr-Coulomb failure criterion, the cohesion (c) and friction angle (φ) of CPB-Rock interface can be directly determined (as shown in Fig. 15).

$$\tau = c + \sigma_c \tan(\varphi) \tag{3}$$

Where τ (kPa) is the shear stress of the CPB-Rock interface, σ_c (kPa) is the confining pressures, c (kPa) and φ (°) are the cohesion and friction angle of the CPB-Rock interface.

There is Fig.15

For the dry rock surface, the cohesion (c) and the friction angle (φ) of the CPB-Rock interface cured for 1 day are 27.01 kPa and 16.17°; while for the wet rock surface, the cohesion (c) and the friction angle (φ) are 9.34 kPa and 19.29°. The data

clearly show that the interfacial cohesion (c) of the dry rock surface is much greater than that of the wet rock surface. However, the interfacial friction angle (φ) of the dry rock surface is slightly less than that of the wet rock surface. The underlying reasons for this will be discussed in the next section.

3.2 Effects of curing time on shear behavior of CPB-Rock interfaces

Fig. 16 shows the curves of Shear stress *vs.* Shear displacement for the CPB-Rock interface with different curing time (1, 3 and 7 days). It evident from Fig.16 that the peak shear stress and shear stiffness increase with a longer curing time. With the same curing time, the interfacial shear strength from the dry rock surface (Fig. 16b) is significantly higher than that of the wet rock surface (Fig. 16a). For the wet rock surfaces, the shear strength increased from 25.79 kPa (for 1 day) to 43.65 kPa (for 7 days). For the dry rock surface, the shear strength increased from 48.32 kPa (for 1 day) to 88.02 kPa (for 7 days). The shear stiffness of the CPB-Rock interface cured for 1, 3, and 7days curing time are 28.57 kPa/mm, 40 kPa/mm, and 65 kPa/mm at the wet rock surface. While for dry rock surfaces, the corresponding shear stiffness are 50 kPa/mm, 83.4 kPa/mm, and 225 kPa/mm. It can be clearly observed that the multi-peak phenomenon shown in Fig. 13b also occurs after 3 and 7 days of curing at the dry rock surface (Fig. 16b).

There is Fig.16

The combined effects of curing time and different rock surface (dry and wet) on the peak stress are shown in Fig. 17. It can be seen from the Fig.17 that the changing trend of the experimental results is consistent regardless of the confining pressure. Therefore, the confining pressure = 150 kPa (Fig. 17d) was chosen to analyze the combined effects of curing time and different rock surface (dry and wet) on the peak stress in the study. With the increases in curing time from 1 to 3 days and 3 to 7 days, the peak shear stress of the CPB-Rock interface increased by 9.68 kPa and 5.17 kPa at the wet rock surface; and by 26.39 kPa and 34.90 kPa at the dry rock surface. This variations in peak shear stress indicated that the curing time has an obvious effect on the shear behavior of the CPB-Rock interface, and the dry rock surface is more sensitive to the curing time than wet rock surface. When the curing time is 1 day, the peak shear stress of the wet rock surface is 13.70% smaller than that of the dry rock surface; when the curing time are 3 and 7 days, the peak shear stresses are 27.02% and 42.52% smaller. It is evident that the longer the curing time the larger the difference in peak shear stress between dry and wet rock surfaces. Collectively, the shear strength of the dry rock surface increased by 86.68% during the curing period from 1 to 7 days, while for the wet rock surface condition the increase is only 19.57% during the same period. The measured data provide clear evidence that the CPB with the dry rock surfaces can provide a stronger binding strength over the CPB with the wet rock surfaces.

There is Fig.17

For both dry and wet rock surfaces, the peak shear stress of the CPB-Rock interface is increased with the curing time. This is thought to be due to a large amount of hydration products (e.g., C-S-H, ettringite, C-H) that were produced to increase the bonding force of the interface. The increase in hydration products with the curing time can be shown through the thermo-gravimetric (TG)/differential thermo-gravimetry (DTG) analyses. The TG/DTG analyses can record the weight loss and thermal decomposition rate under different temperatures (Sha et al., [54]; Lemonis et al., [55]; Haruna and Fall, [56]). In this work, the TG/DTG analyses were performed on the binder pastes (w/c ratio = 1; to simulate the high water content of CPB) using a Netzsch STA449F3 thermal analyzer in a N_2 atmosphere at a heating rate of 10 ℃/min.

The results of TG/DTG analysis for tested samples cured for 1, 3, 7 days were shown in Fig. 18. It is well known that the change in weight at a temperature from 30 ºC to 200 ºC in the TG/DTG analysis is because of the dehydration of ettringite, gypsum and calcium silicate hydrate (C–S–H), which are main products of the binder hydration. And, the weight change at a temperature from 400 ºC to 450 °C is attributed to the disintegration of calcium hydroxide (C-H), which is also the main products of the binder hydration. However, for the weight change at a temperature from 600 ºC to 750 °C, it is attributed to the decomposition of calcium carbonate, which is not the main products of the binder hydration.

As shown in Fig. 18, the TG and DTG curves indicate that the peak and its corresponding weight loss happen at around 110°C and 450°C, and the 7-day curing time resulted the highest peak and weight loss, followed by the 3-day curing time, and 1-day curing time resulted the lowest amount of the two parameters. This demonstrates that the amount of hydration products increases with the curing time. The larger amount of hydration products can not only increase the binding force as well as the shear strength of the CPB-Rock interface, but also can fill the pores at the CPB-Rock interface to increase the contact area at the interface.

There is Fig.18

Fig. 19 shows the typical effects of curing time on shear failure envelopes of the CPB-Rock interface with different rock surface (dry and wet). Regardless the curing time, all the shear failure envelopes of the CPB-Rock interface can be also described by the Mohr-Coulomb failure criterion (Eq. 3). For the dry rock surface (Fig. 19a), with the increases in curing time from 1 day 3 days and 7days, their cohesions (c) are 27.01 kPa, 47.06 kPa and 65.88 kPa, and their friction angles (φ) are 16.17°, 18.42°, and 27.70°, respectively. For the wet rock surface (Fig. 19b), the cohesions (c) are 9.34 kPa, 19.74 kPa and 27.14 kPa; and the friction angle (φ) are 19.29°, 18.77° and 18.26°, respectively.

There is Fig.19

Fig. 20 shows the relationship of shear parameters (the cohesion c & the friction angle φ) with curing time. As shown in the figure, the interfacial cohesion (c) of the wet rock surface is consistently lower than that of the dry rock surface. This difference is caused by the embedding nature of cement particles on dry and wet rock surfaces (*Ref*: Fig. 12). For both dry

and wet rock surfaces, the cohesion (*c*) of the CPB-Rock interface gradually increases with prolonged curing time. This is due to the cement hydration development, a large amount of hydration products (e.g., C-S-H, C-H) were produced to increase the adhesion force of the interface (*Ref*: Fig. 18).

There is Fig.20

However, it is interesting to note that the friction angle (φ) of the dry rock surface is smaller than that of the wet rock surface for 1 day curing time. (shown in Fig. 20). This is because, in a short curing period, once the cement slurry contacts the surface of the dry sandstone, water and cement particles are embedded into the sandstone due to capillary action, causing the air inside the rock to be discharged into the CPB-Rock interface in the form of bubbles. Fig. 21 shows the distribution of surface pores on the CPB (cured for 1 day) shear surface after the shear test for the dry sandstone. As shown in Fig. 21a, there are many pores distributed on the surface of the CPB shear plane. This distribution greatly reduces the contact area between the CPB and the rock surface, thereby greatly reducing the friction angle (φ) of the CPB-Rock interface. It can also be seen from Fig. 21b that the pores at the CPB-Rock interface shows a collapse shape due to the surface tension. The pore morphology indicates that the bubbles are discharged from the interior of the rock to the interface. However, with the increases of curing time, a large amount of hydration products (e.g., C-S-H, C-H) were filled in the bubbles. Therefore, the hydration products will change the size of the bubbles and increase the contact area between the CPB particles and the dry rock surface, thereby increasing the friction angle (φ) of the interface (similar observations were also made by Fang and Fall, [35]). Therefore, after 3-day curing time, the friction angle (φ) of the dry rock interface becomes greater than that of the wet rock surface.

However, for the wet rock surface, the friction angle (φ) of the CPB-Rock interface decreases with the curing time (the extent of reduction is relatively small) due to the water film on the wet rock surface (*Ref*: Fig.5e). As the hydration reaction development, the water film at the interface participates in the hydration reaction, resulting in the occurrence of micro-cracks at the interface (*Ref*: Fig.12b), which led to a slight decrease in the friction angle (φ) of the CPB-Rock interface.

There is Fig.21

4 Conclusions

This study investigated the influence of dry and wet conditions of rock walls on the shear behavior of the CPB-Rock interface and carried out a series of shear tests. The following concluding remarks can be made based on the analysis of the test results:

- The dry or wet condition of the rock wall has an important influence on the shear behavior of the CPB-Rock interface. The test results show that the curing time and the dry or wet condition of the rock surface have significant impacts on the shear strength, friction angle (φ), cohesion (*c)*, and interface failure morphology at the interface.

- On the dry rock surface, due to the capillary phenomenon, the backfill slurry can be embedded inside the rock along the capillary channel. Therefore, the bonding strength (shear strength) is increased by this embedded nature at the CPB-Rock interface. However, under the wet rock wall condition, the bonding strength is greatly reduced due to the presence of water film on the rock surface.
- The shear strength of the CPB-Rock interface under dry rock wall condition is more sensitive to the curing time. And as the curing time increases (from 1 to 7 days), the shear strength of CPB-Rock interface increases for both rock surface conditions (wet and dry). Moreover, the relative differences in shear strength between the wet and dry rock surface conditions are also increased.
- The test results demonstrated that the shear strength criterion is in accordance with the Mohr-Coulomb criterion. The shear parameter of cohesion (c) increases with the increase of curing time and the cohesion (c) for the dry rock condition is consistently higher than that of the wet rock condition. While the share parameter of friction angle (φ) behaves differently, i.e. with the increase of curing time, friction angle decreases slightly for the wet rock surface conditions but increases for the dry rock surface condition. The pore morphology indicated that with longer curing time (i.e. after 3 days) the dry surrounding rock wall will be more conducive to the stability of the filled underground cavities.

The results presented in this study will enhance the understanding of shear behavior of the CPB-Rock interface with different rock surface conditions (wet and dry). And the results demonstrate that the shear strength will be significantly enhanced by improving the dryness of the surrounding rock wall, which is important in the stability of the CPB structure. In case there is water seepage at the surrounding rock walls of the underground cavities (like Fig. 2b), and the rock wall may be in a wet condition, it would be sensible to seal the seepage area first, and then leave the surface of the surrounding rock walls to dry for a period of time before CPB practices. This will effectively improve the stability of the underground CPB structure.

Acknowledgments

This work was conducted with supports from the National Natural Science Foundation of China (Grant Nos. U1602232 and 51474050), the Fundamental Research Funds for the Central Universities (Grant No. N17010829), Doctoral Scientific Research Foundation of Liaoning Province (Grant Nos. 20170540304 and 20170520341). Liaoning Science and Technology Project (2019JH2/10100035), Also, the authors would like to thank PhD. Haiqiang Jiang for supplying the silica tailings and tested molds.

Reference

[1] S.Y. Zhang, L. Yang, F.Y. Ren, J.P. Qiu, H.X. Ding, Rheological and mechanical properties of cemented foam backfill: Effect of mineral admixture type and dosage, Cement. Concrete. Comp. 112 (2020) 103689.

[2] C. Xiao, H.C. Zheng, X.L. Hou, X.J. Zhang, A stability study of goaf based on mechanical properties degradation of rock caused by rheological and disturbing loads, Int. J. Min. Sci. Technol. 25 (5) (2015) 741-747.

[3] E. Yilmaz, Stope depth effect on field behaviour and performance of cemented paste backfills, Int. J. Min. Reclam. Env. 32 (4) (2018) 273-296.

[4] L. Li, P.Y. Yang, A numerical evaluation of continuous backfilling in cemented paste backfilled stope through an application of wick drains, Int. J. Min. Sci. Technol. 25 (6) (2015) 897-904.

[5] S. Cao, W.D. Song, Effect of filling interval time on the mechanical strength and ultrasonic properties of cemented coarse tailing backfill, Int. J. Mineral. Process. 166 (2017) 62-68.

[6] W. Li, P. Ni, Y. Yi, Comparison of reactive magnesia, quick lime, and ordinary Portland cement for stabilization/solidification of heavy metal-contaminated soils, Sci. Total. Environ. 671 (2019.) 741-753.

[7] M. Fall, T. Belem, S. Samb, M. Benzaazoua, Experimental characterization of the stress-strain behaviour of cemented paste backfill in compression, J. Mater. Sci. 42 (11) (2007) 3914-3922.

[8] A. Tariq, E.K. Yanful, A review of binders used in cemented paste tailings for underground and surface disposal practices, J. Environ. Manage. 131 (2013) 138-149.

[9] X. Chen, X.Z. Shi, J. Zhou, Q.S. Chen, E.M. Li, X.H. Du, Compressive behavior and microstructural properties of tailings polypropylene fibre-reinforced cemented paste backfill, Constr. Build. Mater. 190 (2018) 211-221.

[10] M. Fall, M. Benzaazoua, S. Ouellet, Experimental characterisation of the influence of mill tailings fineness and density on the quality of cemented paste backfill, Miner. Eng. 18 (1) (2005) 41-44.

[11] H.Q. Jiang, M. Fall, Y.H. Li, J. Han, An experimental study on compressive behaviour of cemented rockfill, Constr. Build. Mater. 147 (2019) 837-846.

[12] M. Benzaazoua, P. Marion, I. Picquet, B. Bussière, The use of pastefill as a solidification and stabilization process for the control of acid mine drainage, Miner. Eng. 17 (2) (2004) 233-243.

[13] M. Fall, M. Pokharel, Coupled effects of sulphate and temperature on the strength development of cemented tailings backfills: Portland cement-paste backfill, Cement. Concrete. Comp. 32 (10) (2010) 819-828.

[14] Q.S. Chen, Q.L. Zhang, A. Fourie, C. Xin, Utilization of phosphogypsum and phosphate tailings for cemented paste backfill, J. Environ. Manage. 201 (2017) 19-27.

[15] M. Fall, D. Adrien, J.C. Célestin, M. Pokharel, M. Touré, Saturated hydraulic conductivity of cemented paste backfill, Miner. Eng. 22 (15) (2009) 1307-1307.

[16] E. Yilmaz, M. Benzaazoua, T. Belem, B. Bussière, Effect of curing under pressure on compressive strength development of cemented paste backfill. Miner. Eng. 22 (9) (2009) 772-785.

[17] O. Nasir, M. Fall, Shear behaviour of cemented pastefill-rock interfaces, Eng. Geol. 101 (3) (2008) 146-153.

[18] A.X. Wu, Y. Wang, H.J. Wang, S.H. Yin, X.X. Miao, Coupled effects of cement type and water quality on the properties of cemented paste backfill, Int. J. Mineral. Process. 143 (2015) 65-71.

[19] E. Yilmaz, T. Belem, M. Benzaazoua, Specimen size effect on strength of cemented paste backfill subjected to different placement conditions, Eng. Geol. 185 (2015) 52-62.

[20] Z. Lin, C. Guo, D. Cao, P. Ni, F. Wang, An experimental study on the cutting failure of polymer grouting, Constr. Build. Mater. 258 (2020) 119582.

[21] K. Pirapakaran, N. Sivakugan A laboratory model to study arching within a hydraulic fill stope, Geotech. Test. J. 30 (6) (2007) 1-8.

[22] M. Fahey, M. Helinski, A. Fourie, Some aspects of the mechanics of arching in backfilled stopes, Can. Geotech. J. 46 (11) (2009) 1322-1336.

[23] L. Li, M. Aubertin, An analytical solution for the nonlinear distribution of effective and total stresses in vertical backfilled stopes, Int. J. Geomech. Geoeng. 5 (4) (2010) 237-245.

[24] M. Helinski, M. Fahey, A. Fourie, Behavior of cemented paste backfill in two mine stopes: measurements and modeling, J. Geotech. Geoenviron. Eng. 137 (2) (2011) 171-182.

[25] G.S. Liu, L. Li, X.C. Yang, L.J. Guo, A numerical analysis of the stress distribution in backfilled stopes considering nonplanar interfaces between the backfill and rock walls, Int. J. Geotech. Eng. 10 (2016) 271-282.

[26] G.S. Liu, L. Li, X.C. Yang, L.J. Guo, Numerical analysis of stress distribution in backfilled stopes considering interfaces between the backfill and rock walls, Int. J. Geomech.17 (2) (2017) 06016014.

[27] B.X Yan, W.C. Zhu, C. Hou, H.W. Jia, A comparative study on the stress distribution in mine backfill through theoretical and numerical analysis. Journal of Northeastern University Natural Science, 40 (12) (2019) 1773-1778. (in Chinese)

[28] L. Li, J.D. Aubertin, J.S. Dubé, Stress distribution in a cohesionless backfill poured in a silo, Open. Civil. Eng. J. 8 (1) (2014) 1-8.

[29] L. Cui, M. Fall, Multiphysics modeling of arching effects in fill mass, Comput. Geotech. 83 (2017) 114-131.

[30] T. Grice, Recent mine developments in Australia, Proceedings of the 7th International Symposium on Mining with Backfill (MINEFILL). (2001) 351-357

[31] R.J. Mitchell, Model studies on the stability of confined fills, Can. Geotech. J. 26 (2) (1986) 210-216.

[32] K. Fang, M. Fall, Chemically induced changes in the shear behaviour of interface between rock and tailings backfill undergoing cementation, Rock. Mech. Rock. Eng. 52 (9) (2019) 3047-3062.

[33] M. Fall, O. Nasir, Mechanical behaviour of the interface between cemented tailings backfill and retaining structures under shear loads, Geotech. Geol. Eng. 28 (6) (2010) 779–790.

[34] N.J.F. Koupouli, T. Belem, P. Rivard, H. Effenguet, Direct shear tests on cemented paste backfill-rock wall and cemented paste backfill-backfill interfaces, J. Rock. Mech. Geotech. Eng. 8 (4) (2016) 472-479.

[35] K. Fang, M. Fall, Effects of curing temperature on shear behaviour of cemented paste backfillrock interface, Int. J. Rock. Mech. Min. 112 (2018) 184-192.

[36] S.M. Reed, R.N. Singh, Ground water recovery problems associated with opencast mine backfills in the United Kingdom, Int. J. Mine. Water. 5 (3) (1986) 47-74.

[37] S.M. Reed, D.B. Hughes, R.N. Singh, Backfill settlement of restored strip mine sites-case histories, Int. J. Min. Geol. Eng. 5 (2) (1987) 161-169.

[38] H. Nahazanan, S. Clarke, A. Asadi, Z.M. Yusoff, B.K. Huat, Effect of inundation on shear strength characteristics of mudstone backfill, Eng. Geol. 158 (3) (2013) 48-56.

[39] ASTM C143/C143M-15a, Standard Test Method for Slump of Hydraulic-Cement Concrete, ASTM International, West Conshohocken, PA. (2015)

[40] L. Orejarena, M. Fall, The use of artificial neural networks to predict the effect of sulphate attack on the strength of cemented paste backfill, Bull. Eng. Geol. Environ. 69 (4) (2010) 659-670.

[41] W.C. Li, M. Fall, Sulphate effect on the early age strength and self-desiccation of cemented paste backfill, Constr. Build. Mater. 106 (2016) 296-604.

[42] Z.G Xiu, S.H. Wang, Y.C. Ji, F.L. Wang, F.Y. Ren, Experimental investigation on liquefaction and post-liquefaction deformation of stratified saturated sand under cyclic loading, Bull. Eng. Geol. Environ. 79 (5) (2020) 2313-2324.

[43] D.A. Landriault, Paste fill at Inco. In: Proceedings of the 5th International Symposium on Mining with Backfill, Johannesburg: South Africa, (1992) 8.

[44] ASTM D2487-17e1, Standard Practice for Classification of Soils for Engineering Purposes (Unified Soil Classification System), ASTM International, West Conshohocken, PA, 2017.

[45] N. Barton, V. Choubey, The shear strength of rock joints in theory and practice, Rock. Mech. 10 (1-2) (1977) 1-54.

[46] S.G. Du, Y.J. Hu, X.F. Hu, Measurement of joint roughness coefficient by using profilograph and roughness ruler. J. Earth. Sci. 20 (5) (2009) 890-896.

[47] S.G. Du, Y.J. Hu, X.F. Hu, X. Guo, Comparison between empirical estimation by JRC-JCS model and direct shear test for joint shear strength, J. Earth. Sci. 22 (3) (2011) 411-420.

[48] Y.J. Shen, Y.Z. Wang, Y. Yang, Q. Sun, T. Luo, H. Zhang, Influence of surface roughness and hydrophilicity on bonding strength of concrete-rock interface, Constr. Build. Mater. 213 (2019) 156-166.

[49] Y.C. Tian, Q.S. Liu, H. Ma, Q. Liu, P.H. Deng, New peak shear strength model for cement filled rock joints, Eng. Geol. 233 (2018) 269-280.

[50] Q. Zhang, X.C. Li, B. Bai, H.X. Hu, The shear behavior of sandstone joints under different fluid and temperature conditions, Eng. Geol. 357 (2019) 105-143.

[51] T. Belem, A. Harvey, R. Simon, M. Aubertin, Measurement and prediction of internal stresses in an underground opening during its filling with cemented fill, Proceedings of the 5th International Symposium on Ground Support in Mining and Underground Construction. Perth, Australia: Taylor & Francis Group. (2004) 619-630

[52] M. Grabinsky, W.F. Bawden, D. Simon, B. Thompson, In Situ Properties of Cemented Paste Backfill in an Alimak Stope, Canadian Geotechnical Conference, Edmonton. (2008) 790-796.

[53] M. Pokharel, M. Fall, Combined influence of sulphate and temperature on the saturated hydraulic conductivity of hardened cemented paste backfill, Cem. Concr. Compos. 38 (2013) 21-28.

[54] W. Sha, E.A. O'Neill, Z. Guo, Differential scanning calorimetry study of ordinary Portland cement, Cem. Concr. Res. 29 (9) (1999) 1487-1489.

[55] N. Lemonis, P.E. Tsakiridis, N.S. Katsiotis, S. Antiohos, D. Papageorgiou, M.S. Katsiotis, M. Beazi-Katsioti, Hydration study of ternary blended cements containing ferronickel slag and natural pozzolan, Constr. Build. Mater. 81 (11) (2015) 130-139.

[56] S. Haruna, M. Fall, Time- and temperature-dependent rheological properties of cemented paste backfill that contains superplasticizer, Powder. Technol. (360) (2017) 731-740.

Figure Captions

Fig. 1 Schematic diagram of backfilled cavity (adapted from Fang and Fall [32]): (a) the interaction between rock wall and CPB; (b) vertical stress distribution in CPB.

Fig. 2 The pictures for the infiltration of surface water and groundwater into the mine cavity: (a) schematic diagram of dry and wet rock walls; (b) actual infiltration of rock wall.

Fig. 3 The artificial tailings used in this study: (a) the natural state of artificial tailings; (b) its optical microscopic image; (c) the scanning electron microscope (SEM) image (magnified 500 times); (d) its main elements.

Fig. 4 The particle size distribution curves of the silica tailings and the average of 7 mines tailings.

Fig. 5 The rock sample used in this study: (a) the red sandstone; (b) the SEM image (magnified 500 times); (c) the main elements of the red sandstone; (d) the optical microscopic image of the dry red sandstone; (e) the optical microscopic image of the wet red sandstone.

Fig. 6 Point cloud models of the shear surface for the red sandstone sample: (a) the contour of the shear surface; (b) the three-dimensional diagram of the shear surface.

Fig.7 Completed sample (differential settlement can occur during curing process).

Fig. 8 Schematic diagram of: (a) actual diagram of the testing system; (b) schematic diagram of testing specimen.

Fig. 9 The schematic diagram of shear area of the CPB-Rock interface.

Fig.10 Effect of dry and wet rock surfaces on shear behavior of CPB-Rock interface (cured for 1 day; confining pressures = 50 kPa).

Fig. 11 Schematic diagram of different interactions between CPB slurry and rock: (a) on dry sandstone surface. (b) on wet sandstone surface.

Fig. 12 Distribution diagram of calcium element from SEM method: (a) at dry rock surface; (b) at wet rock surface.

Fig. 13 Shear displacement vs Shear stress curves for the CPB-Rock interface under different confining pressures (cured for 1 day): (a) on wet rock surface (WR: wet rock); (b) on dry rock surface (DR: dry rock).

Fig. 14 Fracture morphology of CPB-Rock interfaces after shear tests (cured 1 day; confining pressure = 150 kPa): (a) at wet rock interface; (b) at dry rock interface.

Fig. 15 Peak shear stress versus confining pressure for CPB-Rock interface (cured for 1 day).

Fig. 16 Shear behavior (Shear displacement vs Shear stress) of the CPB-Rock interface under different curing time with confining pressure = 50 kPa: (a) on wet rock surface; (b) on dry rock surface.

Fig. 17 The difference for peak shear stress of CPB-Rock interface between dry and wet rock surfaces with different curing time: (a) confining pressure = 0 kPa; (b) confining pressure = 50 kPa; (c) confining pressure = 100 kPa; (d) confining pressure = 150 kPa.

Fig. 18 Results of TG / DTG analysis for tested samples cured for 1, 3 and 7 days.

Fig. 19 Peak shear stress versus confining pressure for CPB-Rock interface with different curing time: (a) at dry rock surface; (b) at wet rock surface.

Fig. 20 Development of cohesion and friction angle of CPB-Rock interface under different curing time.

Fig.21 The distribution of the pores at the CPB-Rock interface cured for 1day for dry surface: (a) distribution of the pores on the dry CPB-Rock interface; (b) the shape of magnified pore (350 times).

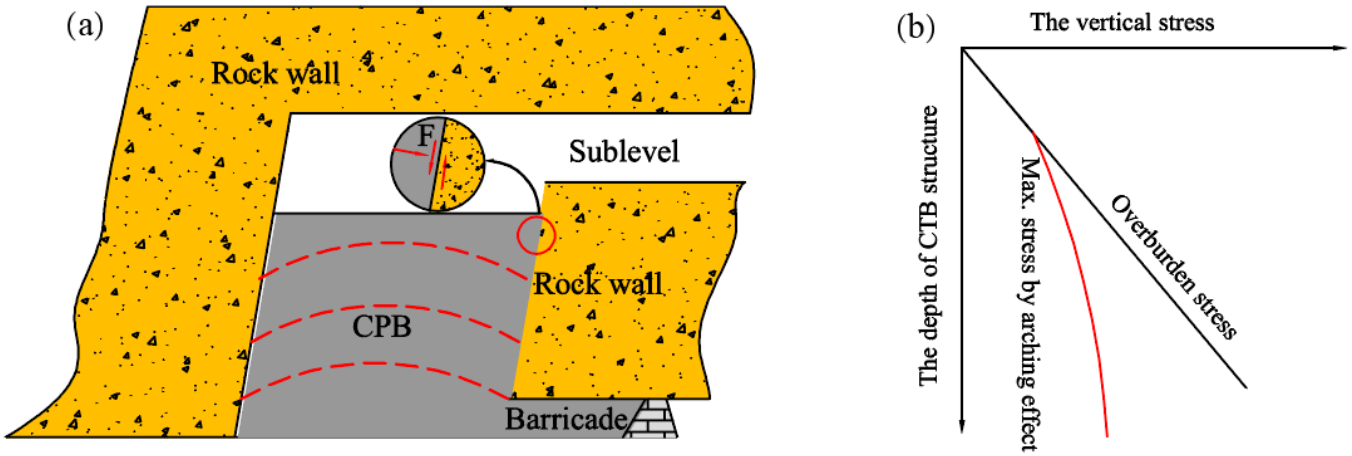

Fig. 1 Schematic diagram of backfilled cavity (adapted from Fang and Fall [32]): (a) the interaction between rock wall and CPB; (b) vertical stress distribution in CPB.

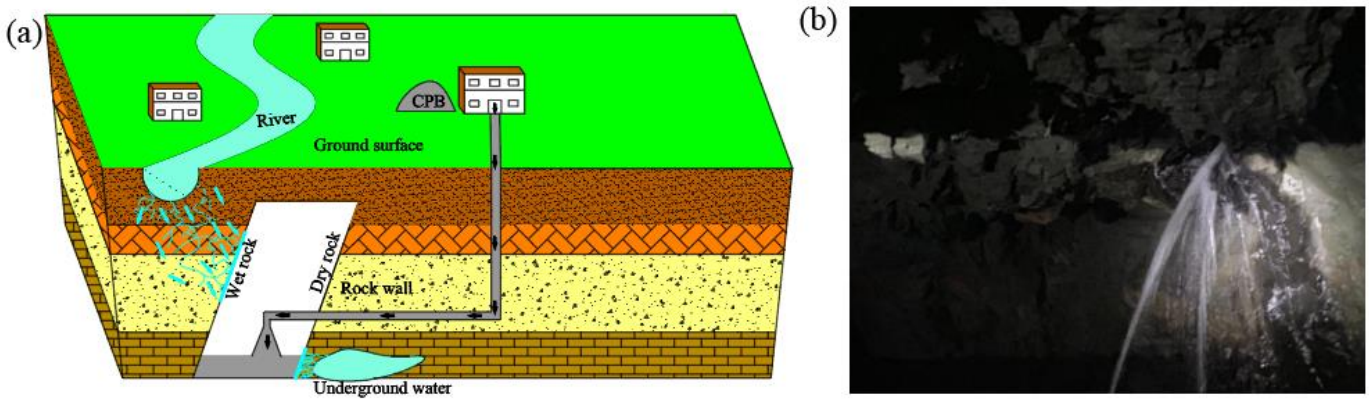

Fig. 2 The pictures for the infiltration of surface water and groundwater into the mine cavity: (a) schematic diagram of dry and wet rock walls; (b) actual infiltration of rock wall.

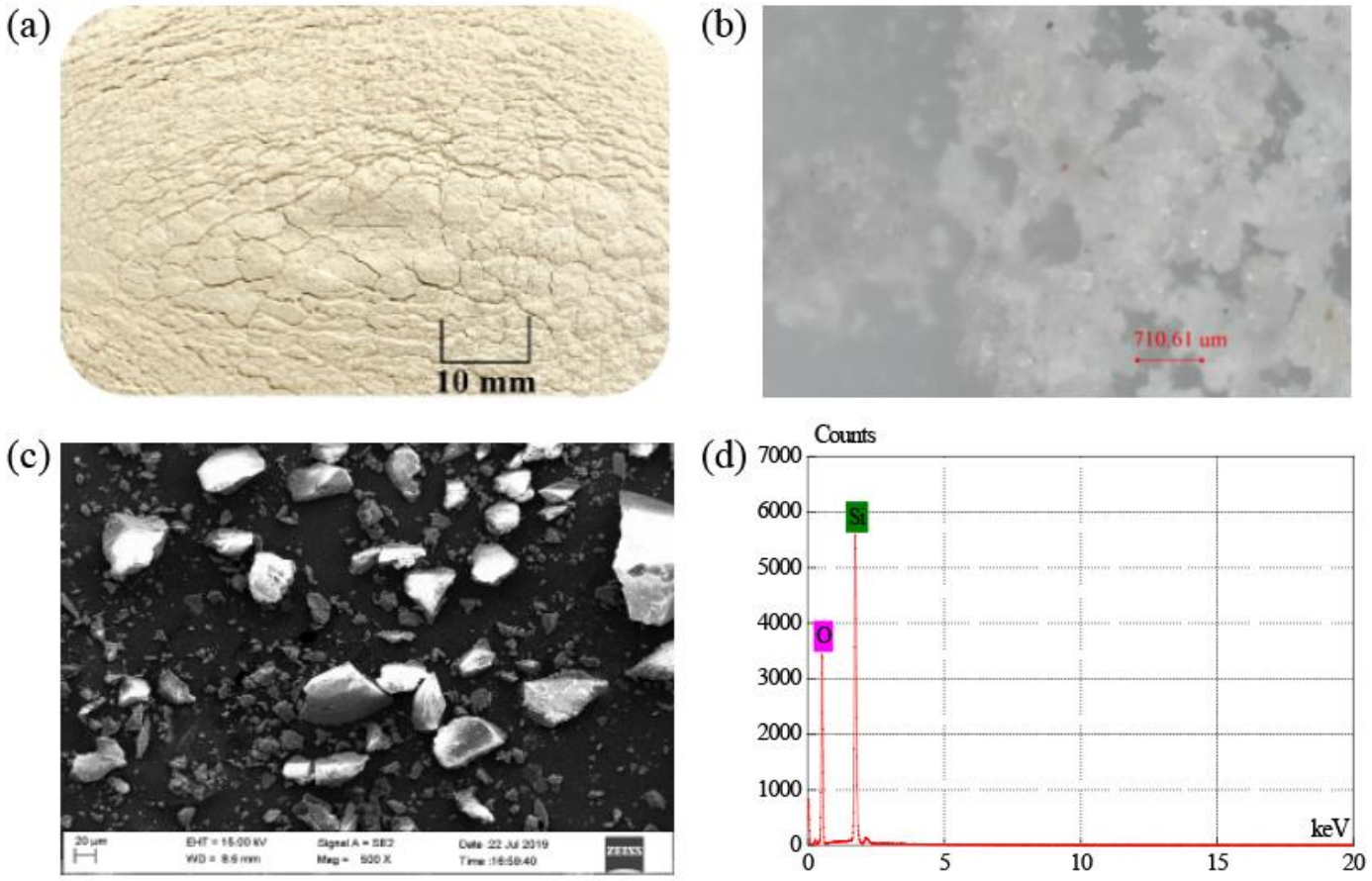

Fig. 3 The artificial tailings used in this study: (a) the natural state of artificial tailings; (b) its optical microscopic image; (c) the scanning electron microscope (SEM) image (magnified 500 times); (d) its main elements.

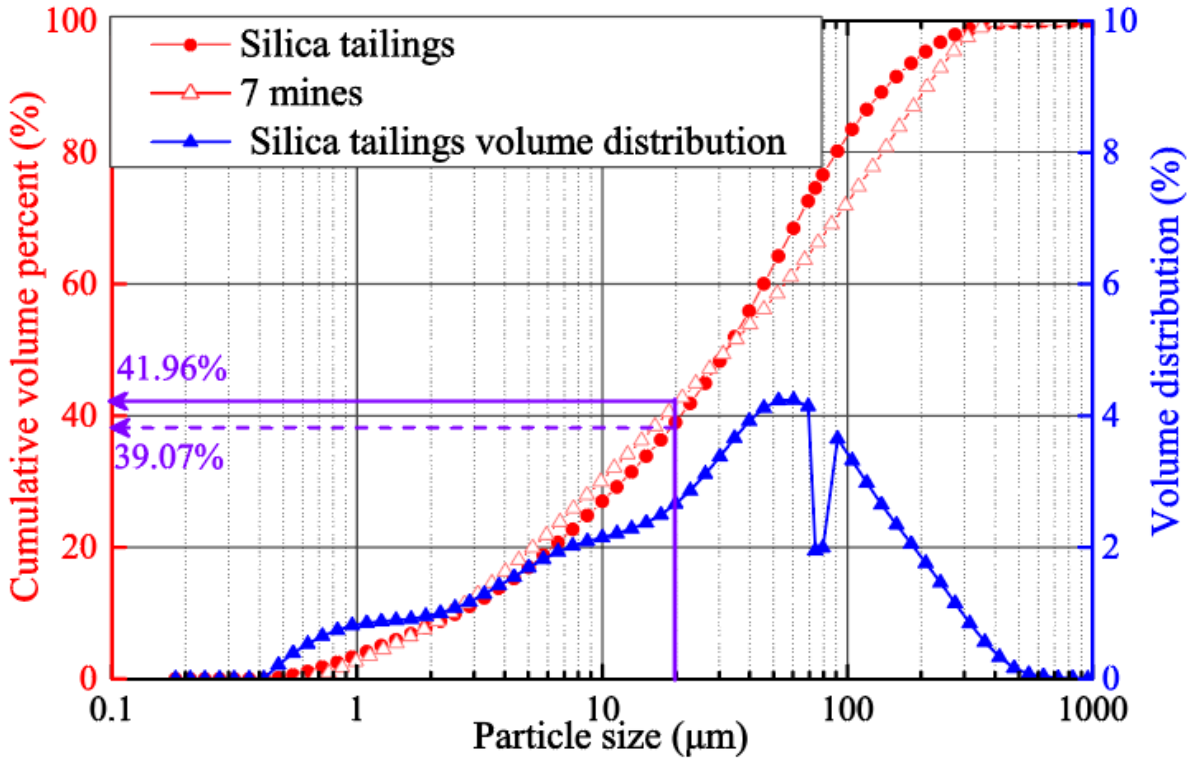

Fig. 4 The particle size distribution curves of the silica tailings and the average of 7 mines tailings.

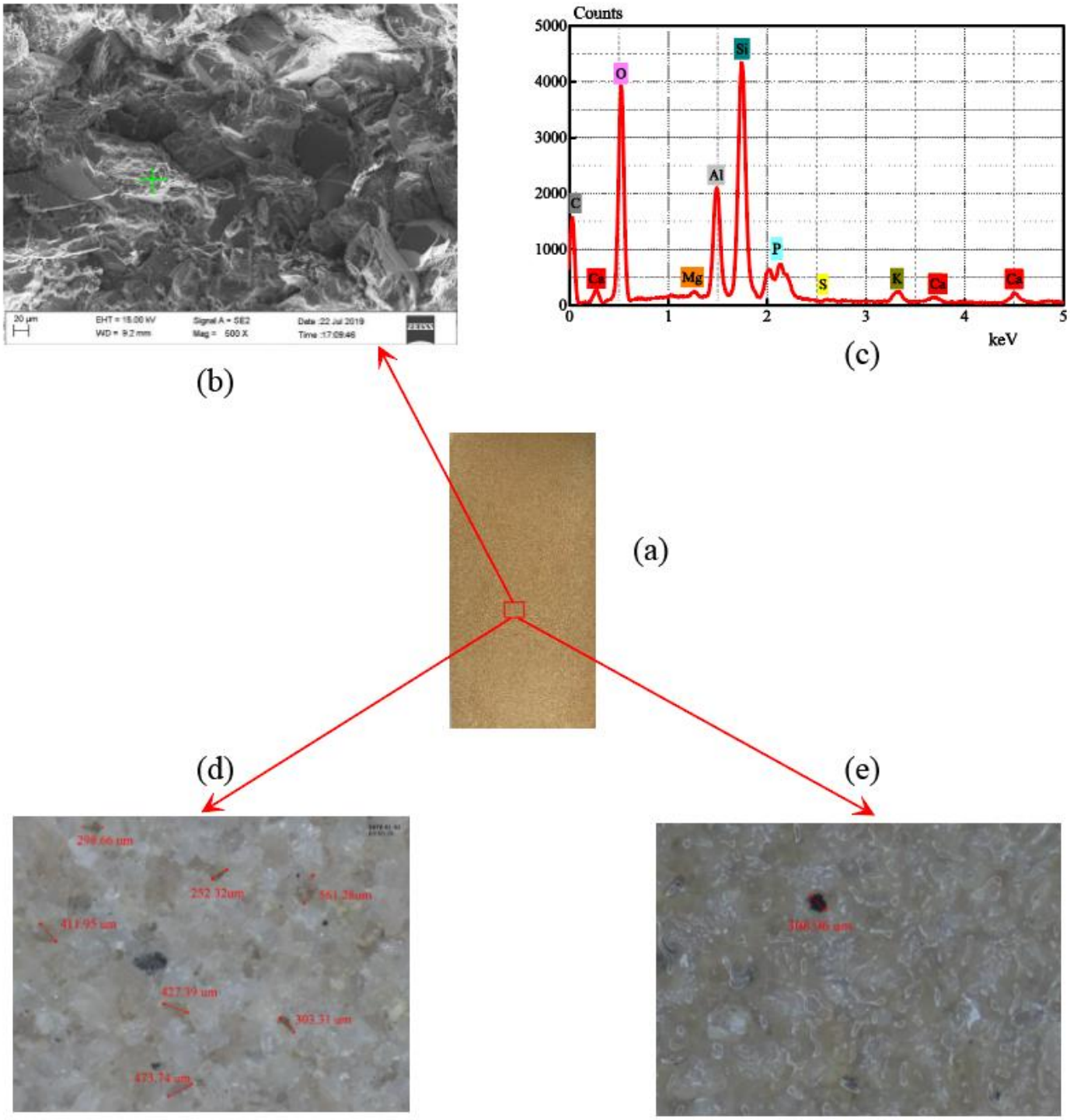

Fig. 5 The rock sample used in this study: (a) the red sandstone; (b) the SEM image (magnified 500 times); (c) the main elements of the red sandstone; (d) the optical microscopic image of the dry red sandstone; (e) the optical microscopic image of the wet red sandstone.

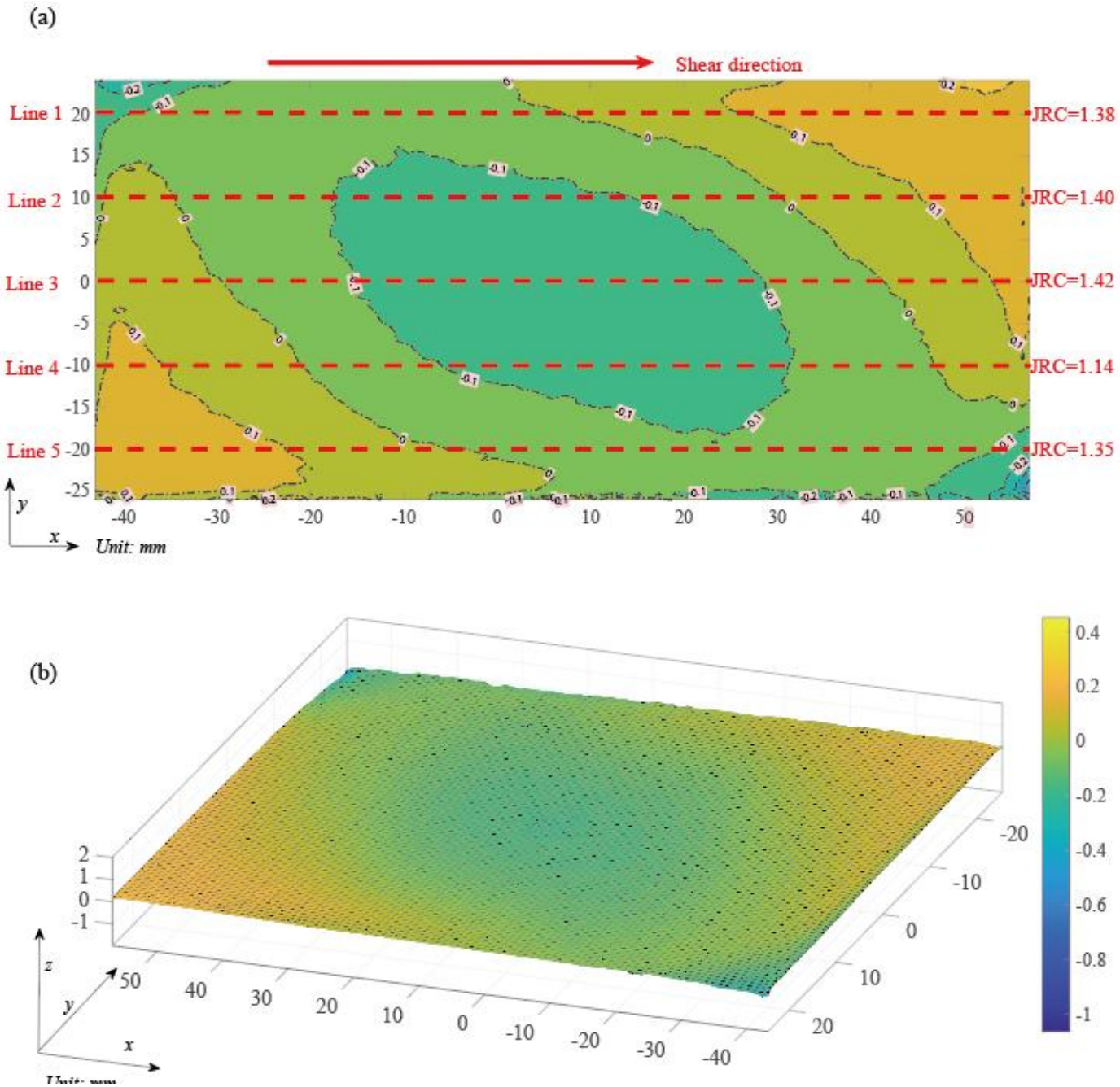

Fig. 6 Point cloud models of the shear surface for the red sandstone sample: (a) the contour of the shear surface; (b) the three-dimensional diagram of the shear surface.

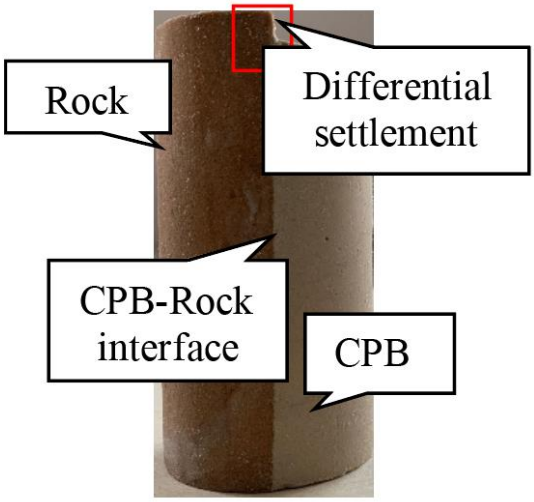

Fig.7 Completed sample (differential settlement can occur during curing process).

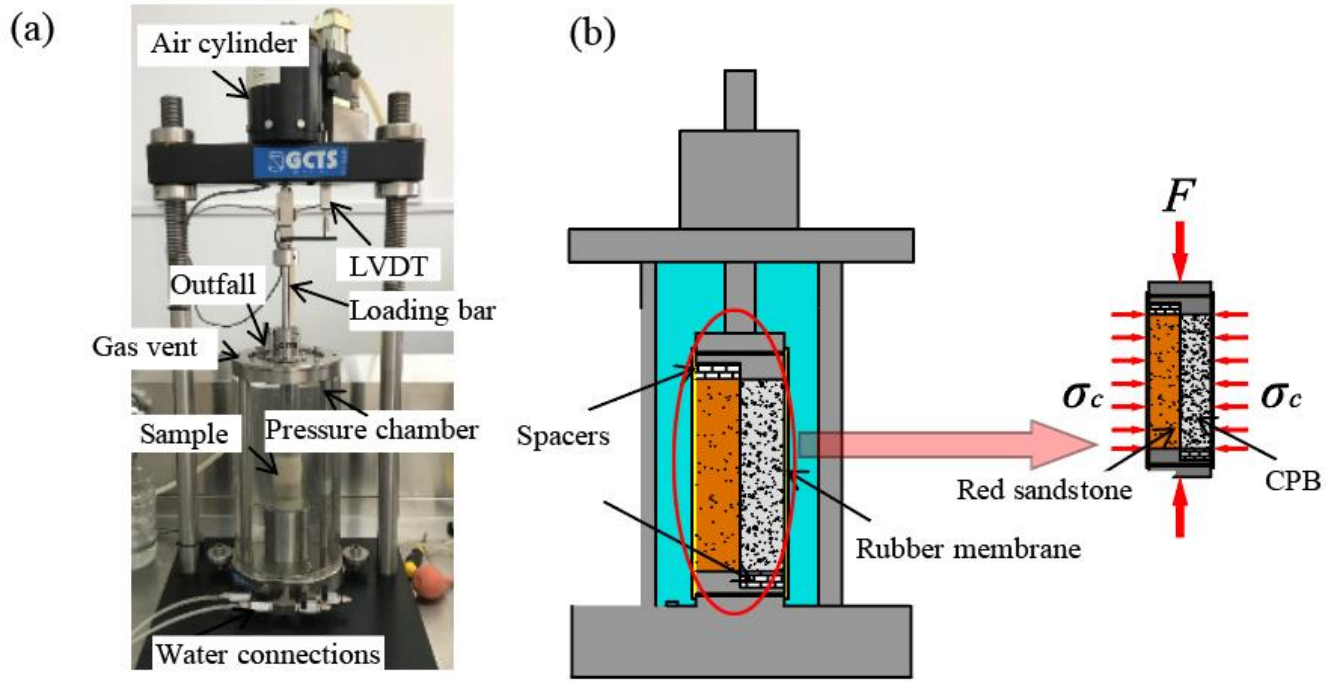

Fig. 8 Schematic diagram of: (a) actual diagram of the testing system; (b) schematic diagram of testing specimen.

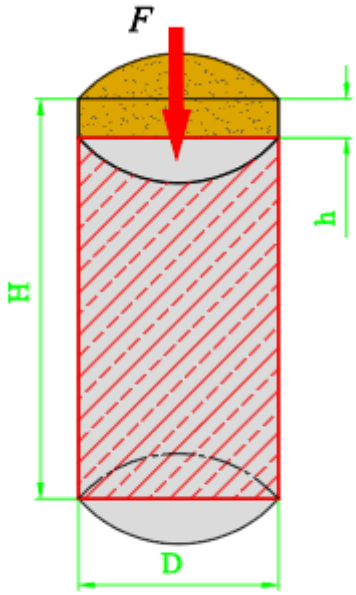

Fig. 9 The schematic diagram of shear area of the CPB-Rock interface.

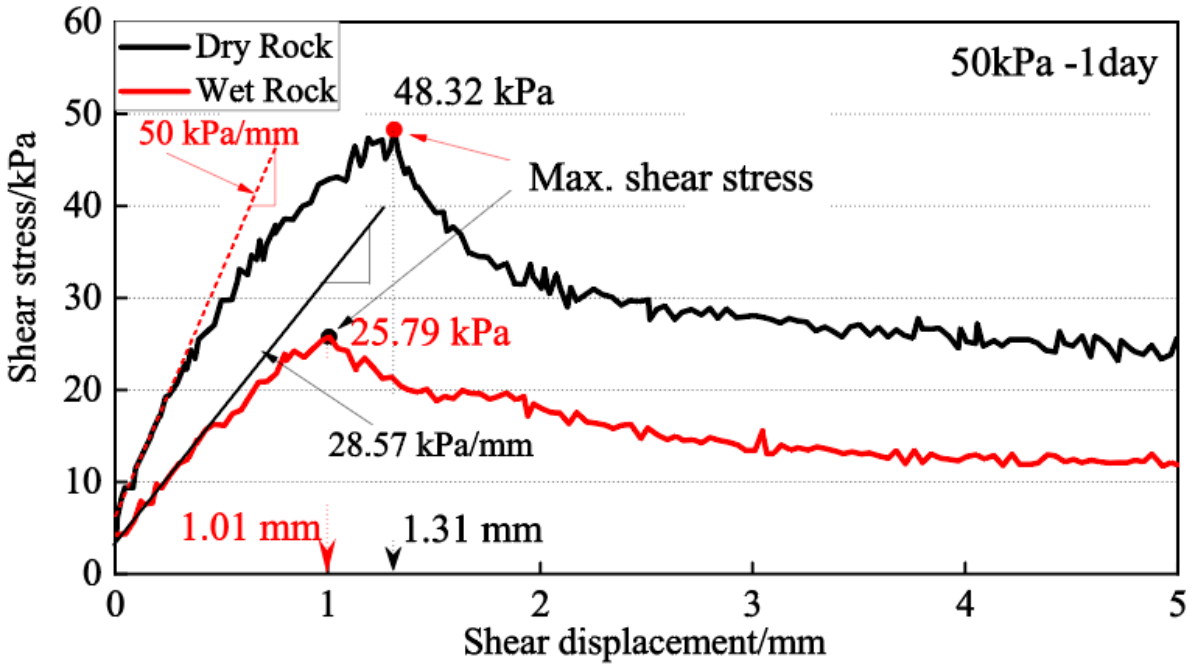

Fig.10 Effect of dry and wet rock surfaces on shear behavior of CPB-Rock interface (cured for 1 day; confining pressures = 50 kPa).

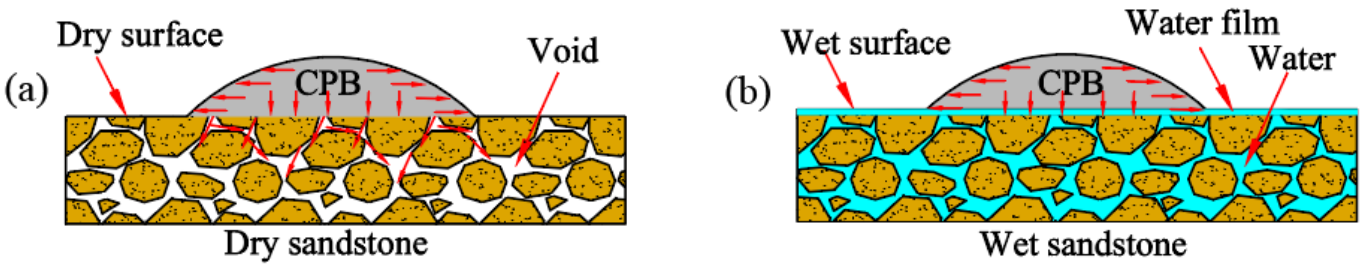

Fig. 11 Schematic diagram of different interactions between CPB slurry and rock: (a) on dry sandstone surface. (b) on wet sandstone surface.

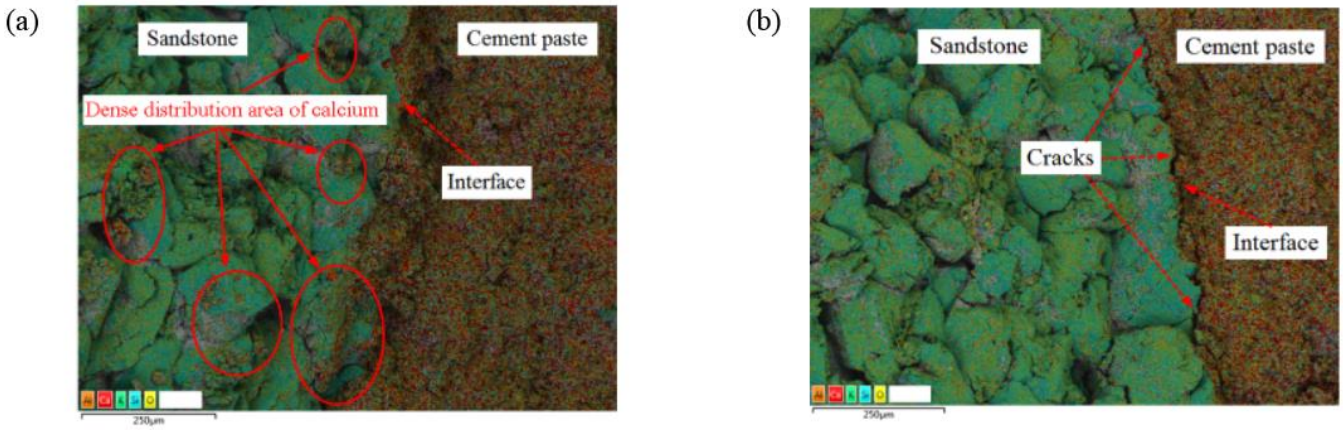

Fig. 12 Distribution diagram of calcium element from SEM method: (a) at dry rock surface; (b) at wet rock surface.

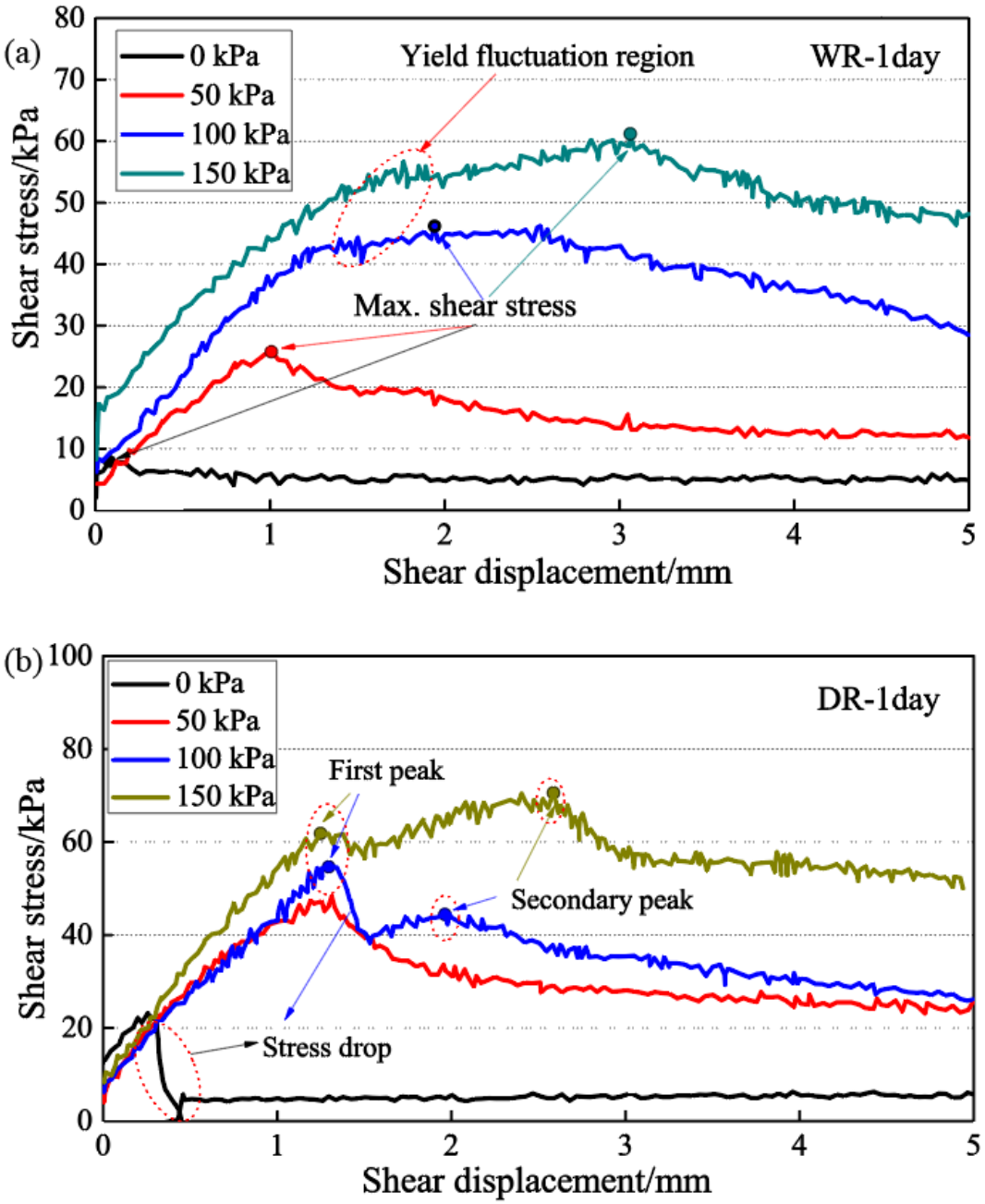

Fig. 13 Shear displacement vs Shear stress curves for the CPB-Rock interface under different confining pressures (cured for 1 day): (a) on wet rock surface (WR: wet rock); (b) on dry rock surface (DR: dry rock).

Fig. 14 Fracture morphology of CPB-Rock interfaces after shear tests (cured 1 day; confining pressure = 150 kPa): (a) at wet rock interface; (b) at dry rock interface.

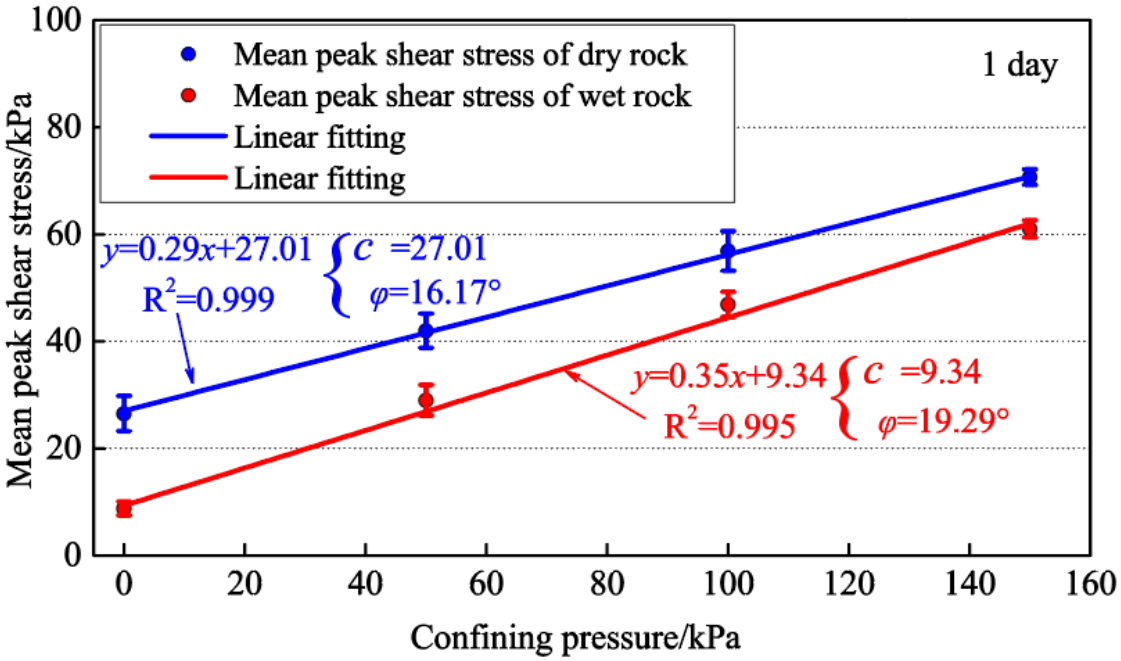

Fig. 15 Peak shear stress versus confining pressure for CPB-Rock interface (cured for 1 day).

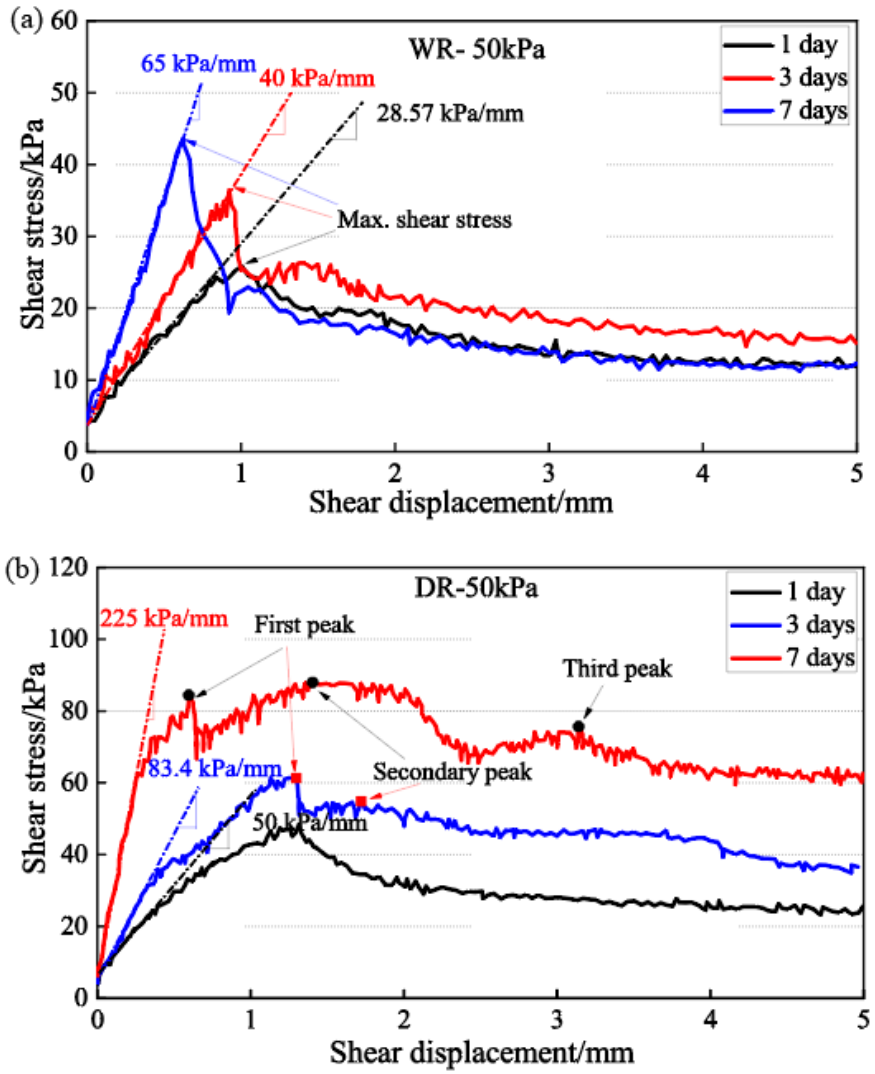

Fig. 16 Shear behavior (Shear displacement vs Shear stress) of the CPB-Rock interface under different curing time with confining pressure = 50 kPa: (a) on wet rock surface; (b) on dry rock surface.

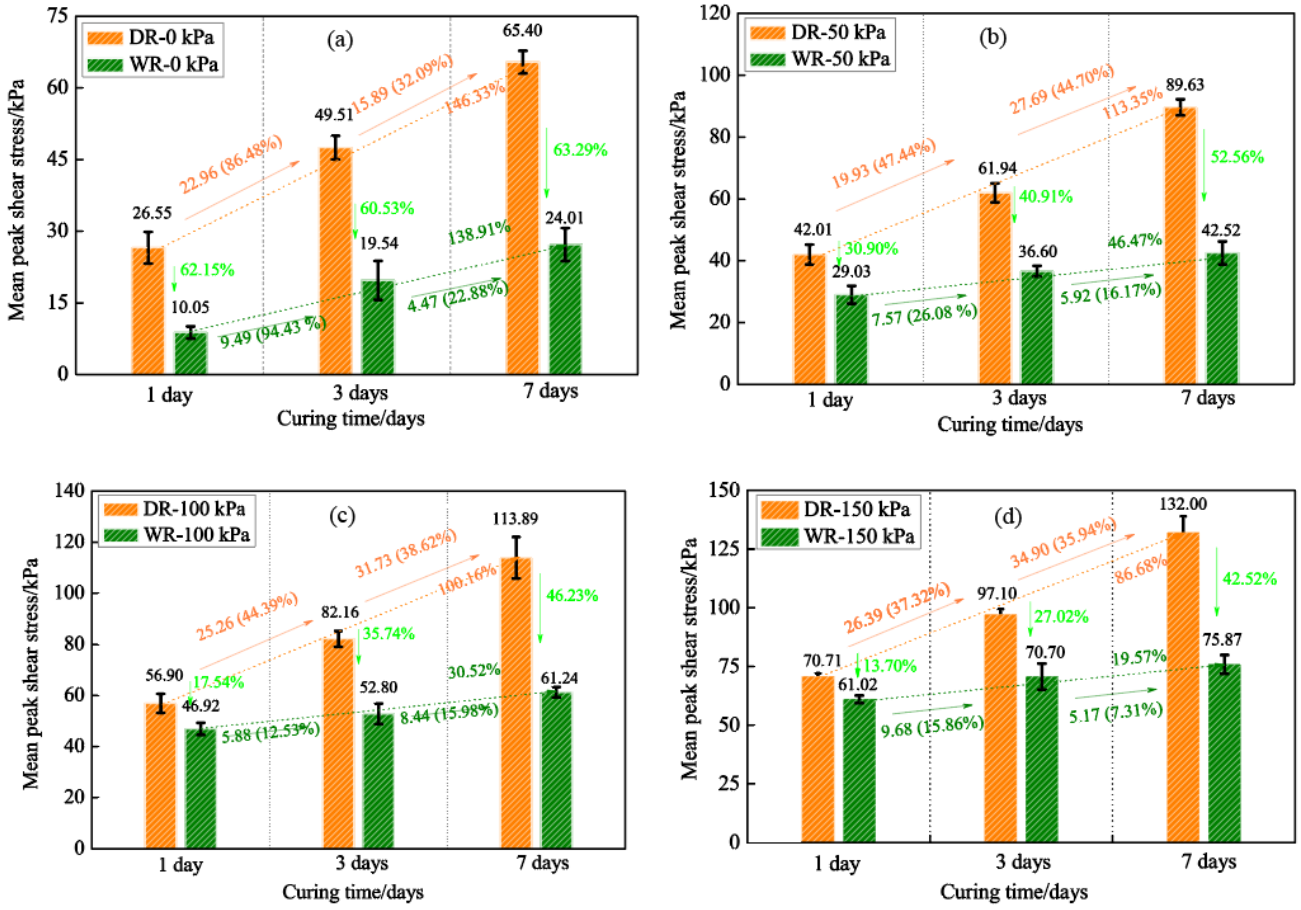

Fig. 17 The difference for peak shear stress of CPB-Rock interface between dry and wet rock surfaces with different curing time: (a) confining pressure = 0 kPa; (b) confining pressure = 50 kPa; (c) confining pressure = 100 kPa; (d) confining pressure = 150 kPa.

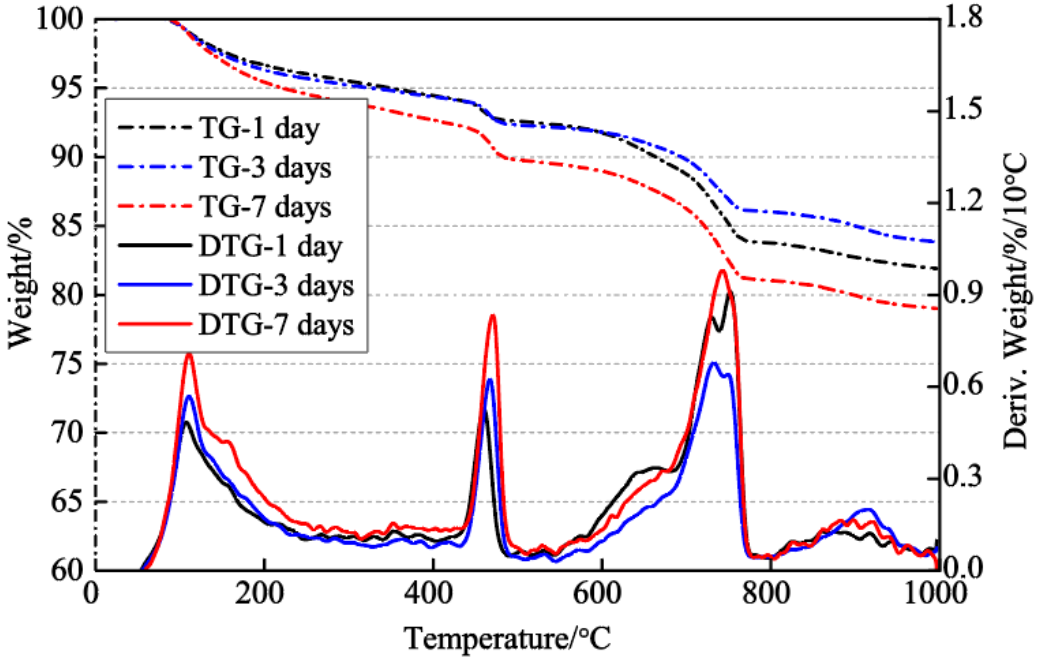

Fig. 18 Results of TG / DTG analysis for tested samples cured for 1, 3 and 7 days.

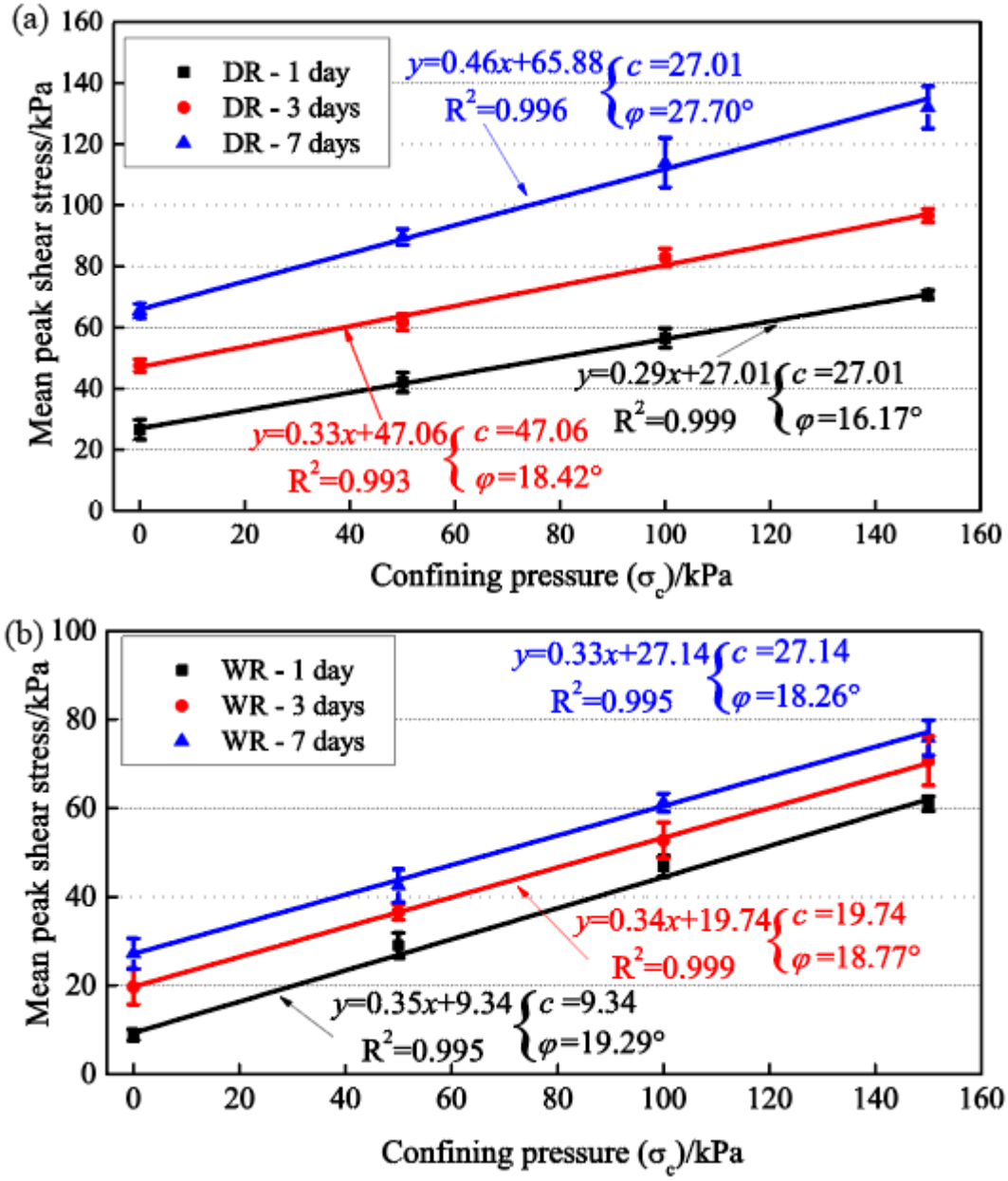

Fig. 19 Peak shear stress versus confining pressure for CPB-Rock interface with different curing time: (a) at dry rock surface; (b) at wet rock surface.

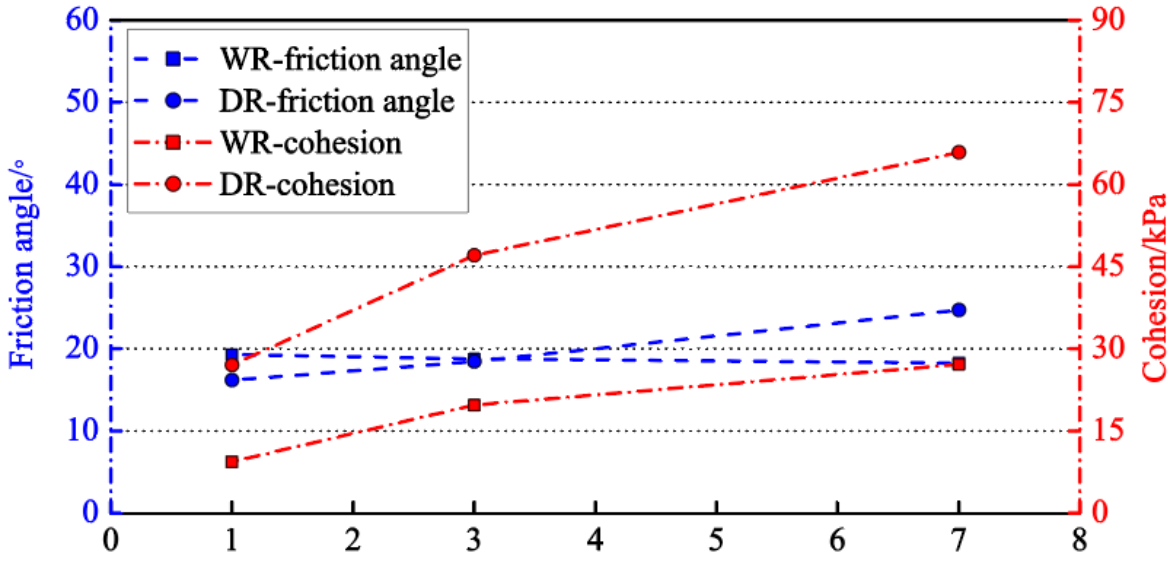

Fig. 20 Development of cohesion and friction angle of CPB-Rock interface under different curing time.

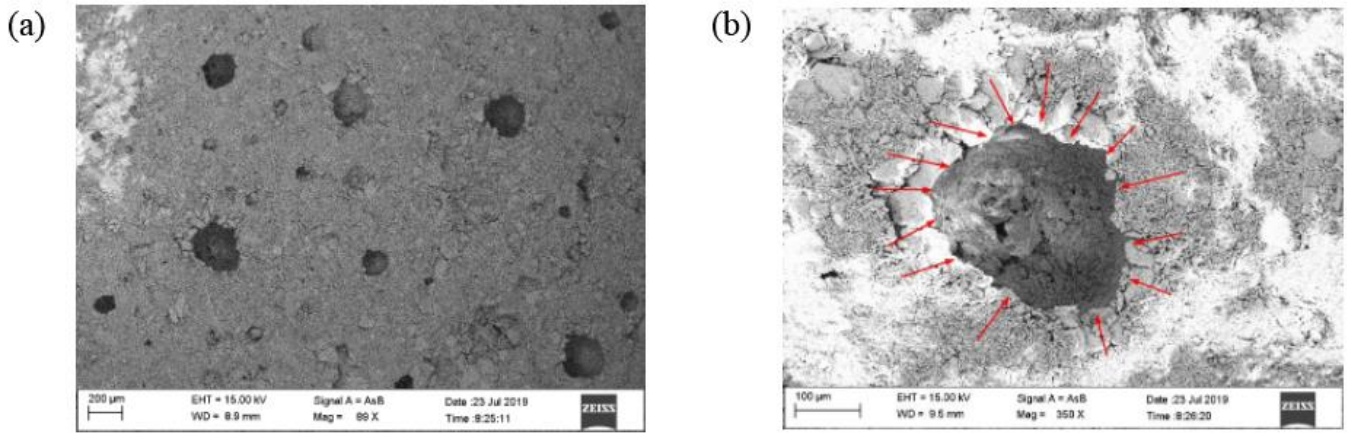

Fig.21 The distribution of the pores at the CPB-Rock interface cured for 1day for dry surface: (a) distribution of the pores on the dry CPB-Rock interface; (b) the shape of magnified pore (350 times).